frontiers in Materials

ORIGINAL RESEARCH
published: 10 December 2021
doi: 10.3389/fmats.2021.792014

Strength Model of Backfill-Rock Irregular Interface Based on Fractal Theory

Yue Zhang[1], *Zhihong Zhang*[1], *Lijie Guo*[2]* *and Xiuli Du*[1]

[1]Key Laboratory of Urban Security and Disaster Engineering, Ministry of Education, Beijing University of Technology, Beijing, China, [2]Beijing General Research Institute of Mining and Metallurgy, Beijing, China

In the two-step open stope subsequent filling mining method, the determination of the strength model for the backfill-rock interface is of great engineering significance to study the stress distribution and stability of the backfill in the stope. Considering the deformation mechanism of the interface and the interaction of the asperities, a strength model for backfill-rock with irregular interface has been proposed based on fractal theory, which can effectively describe the shear mechanical behavior of interfaces with random roughness. The model has been compared with the two-body mechanistic model and good agreements have been achieved. The results show that the shear strength of the interface changes non-linearly with increasing fractal dimension *D*, when the fractal dimension *D* is in the range of 1~1.12. The complete relationship between the interface shear strength and the fractal dimension is given, as the fractal dimension increases from 1 to 2 based on the presented model. At the same time, the quantitative relationship between the interface and backfill friction angles during direct shear testing is analyzed.

Keywords: backfill, irregular interface, strength model, fractal theory, roughness

OPEN ACCESS

Edited by:
John L. Provis,
The University of Sheffield,
United Kingdom

Reviewed by:
Pavlo Maruschak,
Ternopil Ivan Pului National Technical University, Ukraine
Hitoshi Washizu,
University of Hyogo, Japan

***Correspondence:**
Lijie Guo
ljguo264@126.com

Specialty section:
This article was submitted to Structural Materials, a section of the journal Frontiers in Materials

Received: *09 October 2021*
Accepted: *10 November 2021*
Published: *10 December 2021*

Citation:
Zhang Y, Zhang Z, Guo L and Du X (2021) Strength Model of Backfill-Rock Irregular Interface Based on Fractal Theory. Front. Mater. 8:792014. doi: 10.3389/fmats.2021.792014

INTRODUCTION

In recent years, the backfill mining method has been continuously developed (Fall et al., 2005; Ghirian and Fall, 2013; Lingga and Apel, 2018; Jiang et al., 2019) due to its advantages, such as maximizing the rate of ore recovery, improving the safety of the working face, and solving the pollution problem of the tailings pond (Belem and Benzaazoua, 2008; Chen et al., 2018; Tariq and Yanful, 2018). The shear stress between the backfill and surrounding rock reduces part of the self-weight stress, resulting in the arching effect of the backfill (Cui and Fall, 2017; Liu et al., 2017; Fang and Fall, 2019; Fang et al., 2020), as shown in **Figure 1**. The arching effect leads to the redistribution of the backfill internal stress, which has an effect on the stability of the backfill. Therefore, researching the mechanical properties of the interface between backfill and surrounding rock is of great engineering significance.

Numerical simulation is required to more fully reveal the mechanical behavior of the interaction between the backfill and surrounding rock (Sivakugan et al., 2013; Ting et al., 2014; Li and Aubertin, 2015). However, only a few models take the influence of interface elements into account. Liu et al. (2016) investigated the influence of the mechanical interface characteristics on the stress distribution within backfill by setting up boundary elements. However, the interface had a regular saw tooth shape. The roughness of the interface was characterized by the height and angle of the saw teeth. Due to the heterogeneity of rock and the influence of mining and blasting operations, the exposed surface

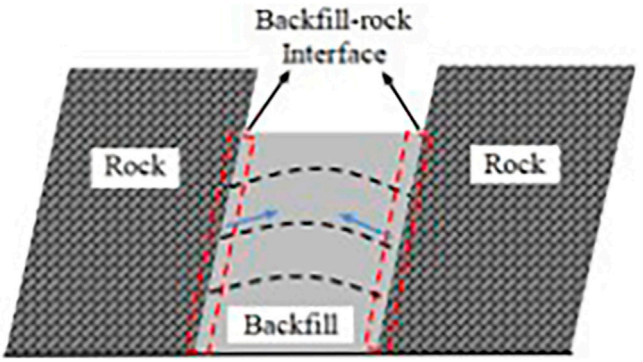

FIGURE 1 | Schematic diagram of the arching effect.

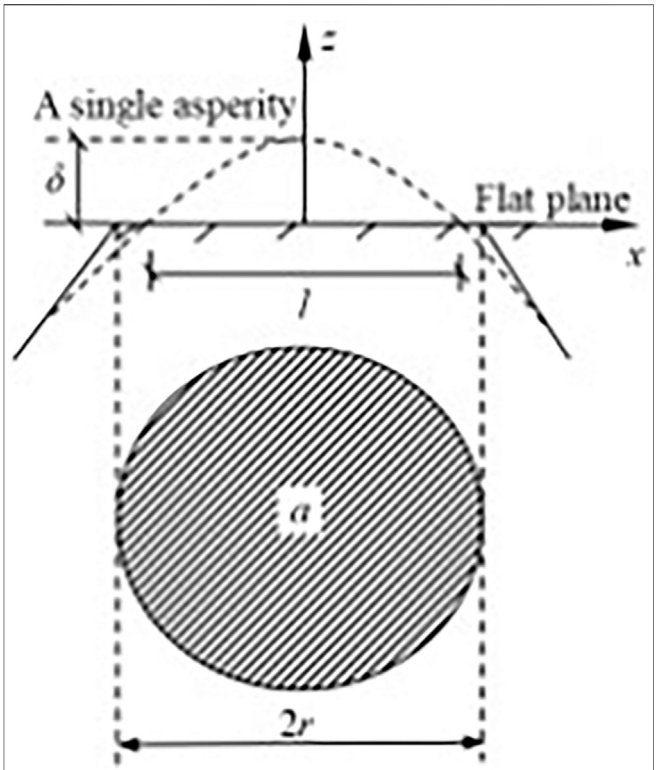

FIGURE 2 | Deformation schematic diagram of a single asperity.

of surrounding rock is usually rough and irregular. At the same time, laboratory tests are an important research method used to reveal the mechanical properties of an interface. Selcuk and Asma (2019), Li et al. (2014), and Wu et al. (2021) carried out uniaxial compression tests and triaxial compression tests to investigate the influence of the interface inclination on the strength and deformation response. Koupouli et al. (2016), Fall and Nasir (2010), Fang and Fall (2018), and Jiang and Fall (2017) obtained qualitative and quantitative relationships between the strength parameters of the backfill-rock interface and backfill under different curing times, curing temperatures and normal stresses by direct shear testing. The laboratory test method can truly reflect the macroscopic mechanical behavior of an interface but ignores the microscopic deformation mechanism of the interface. Therefore, by considering random roughness, establishing an interface strength model is necessary to provide a theoretical basis for further exploring the microscopic deformation mechanism of the interface and more realistically simulating the mechanical properties of the interface.

To solve the contact problem taking into account the microscopic deformation mechanism and irregular roughness, the statistical model and the fractal theoretical model are mainly used. The statistical model uses the parameters that are influenced by the resolution of the measuring device. Thus, the results of the interface characterization and analysis are not unique (Greenwood and Williamson, 1966; Sayles and Thomas, 1978; Carbone, 2009; Beheshti and Khonsari, 2014). Majumdar and Bhushan (1991) proposed an interface contact model based on fractal theory, namely, the M-B fractal model, to overcome the deficiencies of the statistical method. The fractal dimension is used to characterize the random roughness of the interface, and could describe the mechanical characteristics of the material during deformation (Maruschak et al., 2012). But the elastoplastic deformation is not considered in this model. Then, Morag and Etsion (2007) and Liou et al. (2010) modified the model proposed by Majumdar and Bhushan and came to the important conclusion that the deformation of an asperity is first elastic. However, Liu et al. (2015) showed that the deformation of an asperity is first plastic, which is the same as the conclusion of Majumdar and Bhushan. During elastoplastic deformation, the relationship between the contact area and contact load of an asperity is very complicated (Kogut and Etsion, 2002; Jackson and Green, 2003). Therefore, the modified model is controversial.

In this paper, the M-B fractal model is modified based on the proportion of elastic deformation and plastic deformation to better describe the deformation mechanism. The interaction of asperities is described by force analysis. Combined with the Mohr-Coulomb criterion, a strength model of the backfill-rock interface with random roughness is proposed on this basis to further reveal the mechanical behavior of the backfill-rock interface. The relationship between the fractal dimension and the shear strength is also investigated. Finally, the quantitative relationship between the interface and backfill friction angles is presented.

MODELING

Establishment of a Single Asperity Strength Model Based on Fractal Theory

Fractal Model of a Single Asperity

The contact between two rough surfaces can be approximately equivalent to the contact between a rough surface and a rigid smooth flat plane (Majumder and Tien, 1990). From the W-M fractal function, it follows that the profile curve of a single asperity on the backfill surface before deformation can be expressed as (Berry and Lewis, 1980; Mandelbrot, 1985)

$$z(x) = G^{D-1} l^{2-D} \cos \frac{\pi x}{l} \tag{1}$$

where D is the fractal dimension of the rough surface, and $1 < D < 2$; G is the characteristic length scale of the rough surface; l is the base length of an asperity; x is the horizontal distance from any point on the base to the tip of an asperity; and $z(x)$ is the profile curve of a single asperity before deformation.

Figure 2 presents the deformation schematic diagram of a single asperity. The parameters δ, r, and a are the deformation at the tip of an asperity, the microcontact radius, and the microcontact area in **Figure 2**, respectively. Meanwhile, according to the M-B fractal model, the relationship between a and l can be simplified as $l = a^{1/2}$. Then, the deformation and the curvature radius of an asperity are given as follows:

$$\delta = G^{D-1} a^{(2-D)/2} \tag{2}$$

$$R = \frac{1}{G^{D-1} l^{-D} \pi^2} \tag{3}$$

where R is the radius of curvature at the tip of an asperity.

The microcontact area and micro- contact load of an asperity depend on its deformation regime: Elastic, elastoplastic, or plastic.

1) Elastic Deformation

Considering Hertz contact theory (Johnson, 1985), the elastic microcontact area, the elastic microcontact area-load relation, and the maximum microcontact pressure of an asperity are

$$a = \pi R \delta \tag{4}$$

$$F_e = \frac{4E^*}{3\sqrt{\pi}} G^{D-1} a^{\frac{3-D}{2}} \tag{5}$$

$$P_0 = \frac{2E^*}{\pi} \left(\frac{\delta}{R}\right)^{\frac{1}{2}} \tag{6}$$

where E^* is the composite elastic modulus of the interface, and $E^* = (\frac{1-\mu_1^2}{E_1} + \frac{1-\mu_2^2}{E_2})^{-1}$; μ_1, μ_2, E_1, and E_2 are the Poisson's ratios and the elastic moduli of the two microcontact materials, respectively; F_e is the elastic load of an asperity; and P_0 is the maximum microcontact pressure during deformation.

The maximum microcontact pressure is 3/2 times the average microcontact pressure that arises during elastic deformation (Johnson, 1985), namely,

$$P_e = \frac{2}{3} P_0 = \frac{4E^*}{3\pi} \left(\frac{\delta}{R}\right)^{\frac{1}{2}} \tag{7}$$

where P_e is the average elastic microcontact pressure on an asperity.

Without taking friction into account, the critical average pressure of an asperity at the first yield is

$$P_{ec} = 1.1\sigma_y \tag{8}$$

where P_{ec} is the critical average pressure of an asperity, demarcating the elastic and elastoplastic microcontacts, and σ_y is the yield strength of the softer material.

Therefore, the critical microcontact deformation is

$$\delta_{ec} = \left(\frac{3.3\sigma_y \pi}{4E^*}\right)^2 R = \left(\frac{3.3\sigma_y}{4E^*}\right)^2 \frac{\pi a^{D/2}}{G^{D-1}} \tag{9}$$

where δ_{ec} is the critical microcontact deformation of an asperity, demarcating the elastic and elastoplastic deformations.

Then,

$$\frac{\delta_{ec}}{\delta} = \pi \left(\frac{3.3\sigma_y}{4E^*}\right)^2 \left(\frac{a}{G^2}\right)^{D-1} \tag{10}$$

When $\delta = \delta_{ec}$, the critical microcontact area of an asperity at the first yield is obtained as follows:

$$a_{ec} = G^2 \left[\frac{1}{\pi} \left(\frac{4E^*}{3.3\sigma_y}\right)^2\right]^{\frac{1}{D-1}} \tag{11}$$

where a_{ec} is the critical microcontact area of an asperity, demarcating the elastic and elastoplastic microcontact areas.

2) Completely Plastic Deformation.

When an asperity undergoes completely plastic deformation, the microcontact area is equal to the truncated microcontact area (Johnson, 1985), that is,

$$a = 2\pi R \delta \tag{12}$$

At this time,

$$\beta = \frac{E^* r}{\sigma_y R} \approx 30 \tag{13}$$

Thereby,

$$a_{pc} = G^2 \left[\frac{\pi (E^*)^2}{225\sigma_y^2}\right]^{\frac{1}{D-1}} \tag{14}$$

$$\delta_{pc} = G \left[\frac{\pi (E^*)^2}{225\sigma_y^2}\right]^{\frac{2-D}{2D-2}} \tag{15}$$

where a_{pc} is the critical microcontact area of an asperity, which delimits the elastoplastic and plastic microcontact area, and δ_{pc} is the critical microcontact deformation of an asperity, which delimits the elastoplastic and plastic microcontact deformation.

When the average microcontact pressure is equal to $3\sigma_y$, the asperity is in the completely plastic deformation (Johnson, 1985), namely,

$$P_{pc} = P_p = 3\sigma_y \tag{16}$$

where P_{pc} is the critical microcontact pressure of an asperity, demarcating the elastoplastic and plastic microcontacts, and P_p is the average microcontact pressure of an asperity.

In summary, the critical microcontact areas (a_{ec} and a_{pc}) and the critical microcontact deformations (δ_{ec} and δ_{pc}) are independent of the radius of curvature at the tip of an asperity. These parameters relate to only the physical parameters of the materials and the fractal parameters of the surface. In other words, the critical microcontact area and critical microcontact deformation are unique for a rough surface. Then,

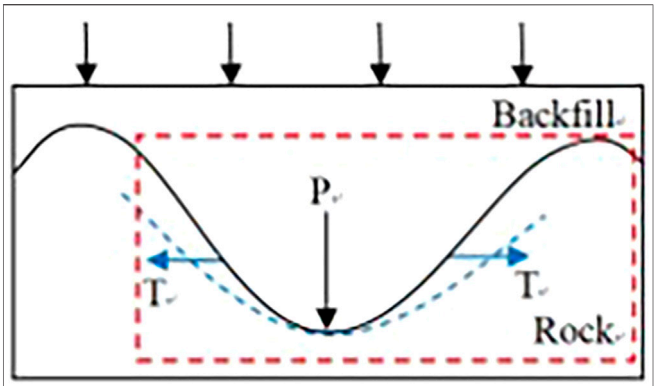

FIGURE 3 | Force schematic diagram of interface under a vertical loading.

the critical microcontact deformations are used to determine the microcontact area and microcontact load of an asperity during elastoplastic deformation.

3) Elastoplastic Deformation

When $\delta_{ec} \le \delta \le \delta_{pc}$, the asperity is in elastoplastic deformation. Considering the proportion of elastic deformation and plastic deformation, the average microcontact pressure is expressed as (Zhao et al., 2000)

$$P_{ep} = 3\sigma_y - 1.9\sigma_y\left(\frac{\ln\delta_{pc} - \ln\delta}{\ln\delta_{pc} - \ln\delta_{ec}}\right) \tag{17}$$

where P_{ep} is the average elastoplastic microcontact pressure on an asperity.

The microcontact area and microcontact load of an asperity are

$$\begin{aligned} a_{ep} &= \pi R\delta + (2\pi R\delta - \pi R\delta) \times \left[-2\left(\frac{\delta - \delta_{ec}}{\delta_{pc} - \delta_{ec}}\right)^3 + 3\left(\frac{\delta - \delta_{ec}}{\delta_{pc} - \delta_{ec}}\right)^2 \right] \\ &= \pi R\delta\left[1 - 2\left(\frac{\delta - \delta_{ec}}{\delta_{pc} - \delta_{ec}}\right)^3 + 3\left(\frac{\delta - \delta_{ec}}{\delta_{pc} - \delta_{ec}}\right)^2\right] \end{aligned} \tag{18}$$

$$\begin{aligned} F_{ep} = P_{ep} \cdot a_{ep} = &\left[3\sigma_y - 1.9\sigma_y\left(\frac{\ln\delta_{pc} - \ln\delta}{\ln\delta_{pc} - \ln\delta_{ec}}\right)\right] \\ &\times \left[1 - 2\left(\frac{\delta - \delta_{ec}}{\delta_{pc} - \delta_{ec}}\right)^3 + 3\left(\frac{\delta - \delta_{ec}}{\delta_{pc} - \delta_{ec}}\right)^2\right] \cdot \pi R\delta \end{aligned} \tag{19}$$

where a_{ep} is the elastoplastic microcontact area of an asperity, and F_{ep} is the elastoplastic microcontact load of an asperity.

In summary, the different deformation regimes of an asperity can be determined by the critical deformation. When $\delta > \delta_{pc}$, an asperity is undergoing completely plastic deformation. When $\delta_{ec} \le \delta \le \delta_{pc}$, an asperity is undergoing elastoplastic deformation. When $\delta < \delta_{ec}$, an asperity is undergoing elastic deformation.

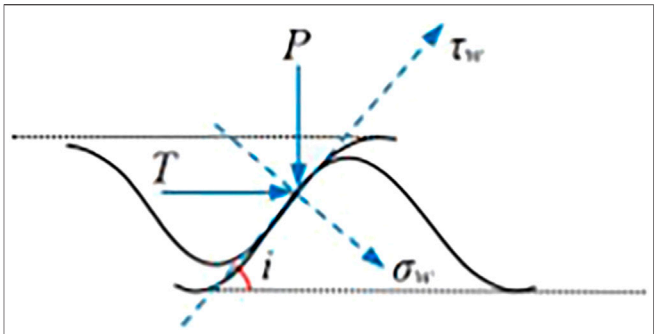

FIGURE 4 | Microcontact stress schematic diagram of two asperities.

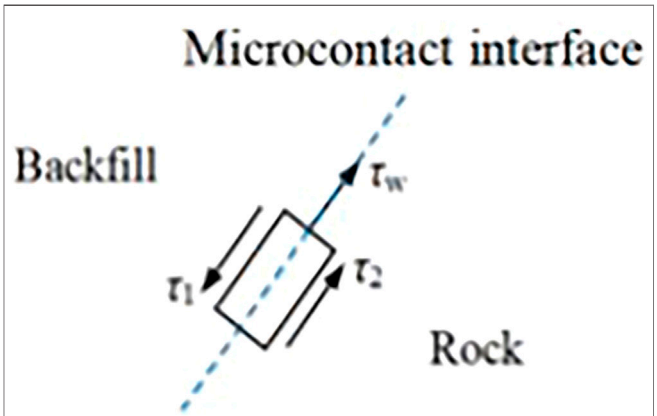

FIGURE 5 | Force schematic diagram of the unit.

Strength Model of a Single Asperity

The M-B fractal model clearly shows that the vertical deformation of an asperity gradually evolves from plastic to elastic deformation. The asperity volume is assumed to remain constant during loading (Hill, 1950), considering the energy conservation theorem. The asperity shape evolves from "tall and thin" to "short and fat", as shown in **Figure 3**. The force p is the vertical external load, and the force T is the horizontal internal force. Thus, the horizontal deformation of an asperity gradually evolves from elastic to plastic.

The dashed box in **Figure 3** is enlarged to analyze the interaction between two asperities during microcontact. The microcontact stress schematic diagram of the two asperities is drawn in **Figure 4**.

Combined with the Mohr-Coulomb criterion, the shear strengths of the microcontact interface, backfill and rock can be expressed as follows:

$$\tau_w = c_w + \sigma_w \tan\varphi_w \tag{20a}$$

$$\tau_1 = c_1 + \sigma_1 \tan(\varphi_1 + i) \tag{20b}$$

$$\tau_2 = c_2 + \sigma_2 \tan\varphi_2 \tag{20c}$$

where τ_w and σ_w are the shear stress and the normal stress of the microcontact interface, respectively; τ_1 and σ_1 are the shear stress

and the normal stress on the shear failure surface of the backfill, respectively; and τ_2 and σ_2 are the shear stress and the normal stress on the shear failure surface of the rock, respectively. Adhesion is defined as the ability of one material to adhere to the surface of another material (Luo et al., 2017). Cohesion is defined as the ability of adjacent parts of the same material to attract each other. Thus, c_w is defined as the adhesion of the microcontact interface; c_1 and c_2 are the cohesion of the backfill and rock, respectively; φ_w is the friction angle of the microcontact interface; φ_1 and φ_2 are the friction angles of backfill and rock, respectively; and i is the inclined angle of the asperities on the rock surface to impede the movement of the asperities on the backfill surface.

A unit on the microcontact interface in **Figure 4** is taken for force analysis, as shown in **Figure 5**. According to **Figure 5**, the static equilibrium equations of the unit are established for different deformation regimes. The relationships of the strength parameters between the microcontact interface and backfill in different deformation regimes are solved.

1) Elastic Deformation

When the asperity on the backfill surface is undergoing elastic deformation, the normal stress on the microcontact interface is $\sigma_w = \sigma_1 = \sigma_2 = P_e$. The shear strength of the interface is mainly determined by the backfill, namely, $\tau_w = \tau_1$. Then, the cohesion and friction angle of the microcontact interface are

$$\begin{cases} c_w = c_1 \\ \varphi_w = \varphi_1 + i \end{cases} \tag{21}$$

2) Elastoplastic Deformation

When the asperity on the backfill surface is undergoing elastoplastic deformation, the normal stress on the microcontact interface is $\sigma_w = \sigma_1 = \sigma_2 = P_{ep}$. The shear strength is mainly determined by the backfill and rock, namely, $\tau_w = \tau_2 - \tau_1$. Then, the cohesion and friction angle of the microcontact interface are

$$\begin{cases} c_w = c \\ \tan\varphi_w = \tan\varphi_2 - \tan(\varphi_1 + i) \end{cases} \tag{22}$$

where $0 < c < c_1$.

3) Completely Plastic Deformation

When the asperity on the backfill surface is undergoing completely plastic deformation, the normal stress on the microcontact interface is $\sigma_w = \sigma_1 = \sigma_2 = P_p$. The shear strength is mainly determined by the backfill and rock, namely, $\tau_w = \tau_2 - \tau_1$. Then, the cohesion and friction angle of the microcontact interface are

$$\begin{cases} c_w = 0 \\ \tan\varphi_w = \tan\varphi_2 - \tan(\varphi_1 + i) \end{cases} \tag{23}$$

Establishment of the Interface Strength Model Based on Fractal Theory

Fractal Model of the Irregular Interface

In different deformation regimes, the contact area and contact load are related to the deformation of the largest microcontact when the two rough surfaces are in contact.

1) Completely Plastic Deformation

If $a_L < a_{pc}$, all the asperities on the backfill surface are undergoing completely plastic deformation. At this time, the size distribution of the microcontact areas is as follows:

$$n(a) = \frac{D}{2}\psi^{(2-D)/2}(a_L)^{D/2}(a)^{-(D+2)/2} \tag{24}$$

where a_L is the largest microcontact area of the interface and $n(a)$ is the size distribution of the microcontact areas under completely plastic and elastoplastic deformation.

Then, the plastic contact area and contact load can be given by

$$A_{rp} = \int_0^{a_{pc}} n(a)ada = \frac{D}{2-D}\psi^{\frac{2-D}{D}}(a_L)^{\frac{D}{2}}\left(a_{pc}\right)^{\frac{2-D}{2}} \tag{25}$$

$$F_{cp} = \int_0^{a_{pc}} P_p an(a)da = 3\sigma_y\frac{D}{2-D}\psi^{\frac{2-D}{D}}(a_L)^{\frac{D}{2}}\left(a_{pc}\right)^{\frac{2-D}{2}} \tag{26}$$

where A_{rp} and F_{cp} are the contact area and contact load of the interface, respectively, during completely plastic deformation only.

2) Elastoplastic Deformation

The interface contact area and contact load during elastoplastic deformation are solved by the critical microcontact area and critical microcontact deformation of the different deformation regimes. If $a_{pc} \le a_L \le a_{ec}$ and $\delta_{pc} \le \delta \le \delta_{ec}$, all the asperities on the backfill surface are undergoing elastoplastic deformation. The elastoplastic contact area and contact load are expressed as follows:

$$A_{rep} = \int_{a_{pc}}^{a_{ec}} n(a)ada = \frac{D}{2-D}\psi^{\frac{2-D}{D}}(a_L)^{\frac{D}{2}}\left[(a_{ec})^{\frac{2-D}{2}} - \left(a_{pc}\right)^{\frac{2-D}{2}}\right] \tag{27}$$

$$\begin{aligned} F_{cep} &= \int_{a_{pc}}^{a_{ec}}\int_{\delta_{pc}}^{\delta_{ec}} F_{ep}n(a)d\delta da \\ &= \int_{a_{pc}}^{a_{ec}}\int_{\delta_{pc}}^{\delta_{ec}}\left[3\sigma_y - 1.9\sigma_y\left(\frac{\ln\delta_{pc} - \ln\delta}{\ln\delta_{pc} - \ln\delta_{ec}}\right)\right] \\ &\quad \times\left[1 - 2\left(\frac{\delta - \delta_{ec}}{\delta_{pc} - \delta_{ec}}\right)^3 + 3\left(\frac{\delta - \delta_{ec}}{\delta_{pc} - \delta_{ec}}\right)^2\right]\cdot\pi R\delta\cdot n(a)d\delta da \\ &= 2\int_{a_{pc}}^{a_{ec}}\int_{\delta_{pc}}^{\delta_{ec}}\left[3\sigma_y - 1.9\sigma_y\left(\frac{\ln\delta_{pc} - \ln\delta}{\ln\delta_{pc} - \ln\delta_{ec}}\right)\right] \\ &\quad \times\left[1 - 2\left(\frac{\delta - \delta_{ec}}{\delta_{pc} - \delta_{ec}}\right)^3 + 3\left(\frac{\delta - \delta_{ec}}{\delta_{pc} - \delta_{ec}}\right)^2\right] \\ &\quad \cdot a\cdot\frac{D}{2}\psi^{(2-D)/2}(a_L)^{D/2}(a)^{-(D+2)/2}d\delta da \end{aligned} \tag{28}$$

where A_{rep} and F_{cep} are the contact area and contact load of the interface, respectively, during elastoplastic deformation only.

3) Elastic Deformation

If $a_L > a_{ec}$, all the asperities on the backfill surface are undergoing elastic deformation. The size distribution of the microcontact areas is as follows:

$$n(a) = \frac{D}{2}(a_L)^{D/2}(a)^{-(D+2)/2} \tag{29}$$

where $n(a)$ is the size distribution of the microcontact areas during elastic deformation.

Then, the plastic contact area and contact load are expressed as follows:

$$A_{re} = \int_{a_{ec}}^{a_L} n(a)ada = \frac{D}{2-D}(a_L)^{\frac{D}{2}}\left[(a_L)^{\frac{2-D}{2}} - (a_{ec})^{\frac{2-D}{2}}\right] \tag{30}$$

If $1 < D < 2$ and $D \neq 1.5$,

$$F_{ce} = \int_{a_{ec}}^{a_L} F_e n(a)da = \frac{4E^* DG^{D-1}a_L^{\frac{D}{2}}}{3\sqrt{\pi}(3-2D)}\left[(a_L)^{\frac{3-2D}{2}} - (a_{ec})^{\frac{3-2D}{2}}\right] \tag{31a}$$

Similarly, if $D = 1.5$,

$$F_{ce} = \int_{a_{ec}}^{a_L} F_e n(a)da = \frac{1}{\sqrt{\pi}}E^* G^{\frac{1}{2}}a_L^{\frac{3}{4}}(\ln a_L - \ln a_{ec}) \tag{31b}$$

where A_{re} and F_{ce} are the contact area and contact load of the interface, respectively, during elastic deformation only.

Strength Model of the Irregular Interface

A contact strength model of the interface is established by analyzing the strength model parameters of a single asperity.

1) Elastic Deformation.

The shear strength of the interface can be expressed as follows:

$$\tau_{we} = c_1 + \frac{F_{ce}}{A_{re}}\tan(\varphi_1 + \bar{i}) \tag{32}$$

where $\bar{i}$ is the average inclined angle of the asperities on the rock surface and τ_{we} is the shear strength of the interface during elastic deformation only.

2) Elastoplastic Deformation

The shear strength of the interface can be given by

$$\tau_{wep} = c + \frac{F_{cep}}{A_{rep}}\left[\tan\varphi_2 - \tan(\varphi_1 + \bar{i})\right] \tag{33}$$

where τ_{we} is the shear strength of the interface during elastoplastic deformation only.

3) Completely Plastic Deformation

The shear strength of the interface is

$$\tau_{wp} = \frac{F_{cp}}{A_{rp}}\left[\tan\varphi_2 - \tan(\varphi_1 + \bar{i})\right] \tag{34}$$

where τ_{wp} is the shear strength of the interface during completely plastic deformation only.

Therefore, the total shear strength of the interface is

$$\tau_w = c_1 + \left\{\begin{array}{l} \frac{F_{ce}}{A_{re}}\tan(\varphi_1 + \bar{i}) \\ +\frac{F_{cep}}{A_{rep}}\left[\tan\varphi_2 - \tan(\varphi_1 + \bar{i})\right] \\ +\frac{F_{cp}}{A_{rp}}\left[\tan\varphi_2 - \tan(\varphi_1 + \bar{i})\right] \end{array}\right\} \tag{35}$$

where τ_w is the total shear strength of the interface.

Eq. 35 indicates that the shear strength of the interface is determined by the adhesion and friction. To ensure the stability of the backfill-rock interface, the maximum adhesion (namely, c_1) during deformation is taken as the total adhesion of the interface in **Eq. 35**. The total friction of the interface is the sum of all the frictions corresponding to different deformation regimes.

Meanwhile, the relationship among the parameters can be obtained as:

$$\left(P_e + P_{ep} + P_p\right)\tan\varphi_w = P_e\tan(\varphi_1 + \bar{i}) + \left(P_{ep} + P_p\right)\left[\tan\varphi_2 - \tan(\varphi_1 + \bar{i})\right] \tag{36}$$

VERIFICATION

Liu et al. (2005) investigated the effect of the interface roughness on the shear strength by the two-body mechanistic model. Based on this work, the presented model is verified in this section. The yield strength of the concrete is chosen to 3 MPa. The characteristic length scale of the rough surface is chosen to 10^{-11} m. The material parameters are shown in **Table 1**.

Figure 6 shows the verification diagram of the relationship between the shear strength and the fractal dimension. The shear strengths of the presented model and the two-body mechanistic model are normalized to further comparatively analyze the evolution laws between the shear strength and the fractal dimension of the newly presented model and the two-body mechanistic model. The trends of the two models have good agreements, namely, the shear strength changes non-linearly with increasing fractal dimension. The shear strength increases with increasing fractal dimension when $D < 1.095$, peaks at $D = 1.095$ and decreases when $D > 1.095$, which is the same as the evolution laws presented by Liu. Analysis suggests that it is related to the main dislocation form of the asperities on the interface. It should be noted that increasing the fractal dimension corresponds to increasing the distribution density of the asperities on the interface, namely, increasing the frequency of the asperities for the same amplitude. The forms of dislocation between two asperities are sliding, interlocking, and shearing. Some small asperities merge with each other to form large asperities with

TABLE 1 | Material parameters.

Material	Elastic modulus *E*/GPa	Poisson's ratio μ	Cohesion φ/(°)	Internal friction angle *c*/MPa
Concrete	26	0.167	25	3
Rock	35	0.220	35	2

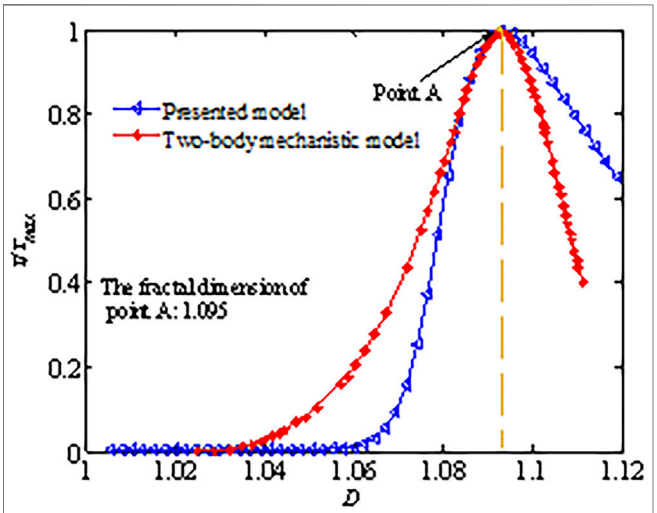

FIGURE 6 | Verification diagram of the relationship between the shear strength and the fractal dimension.

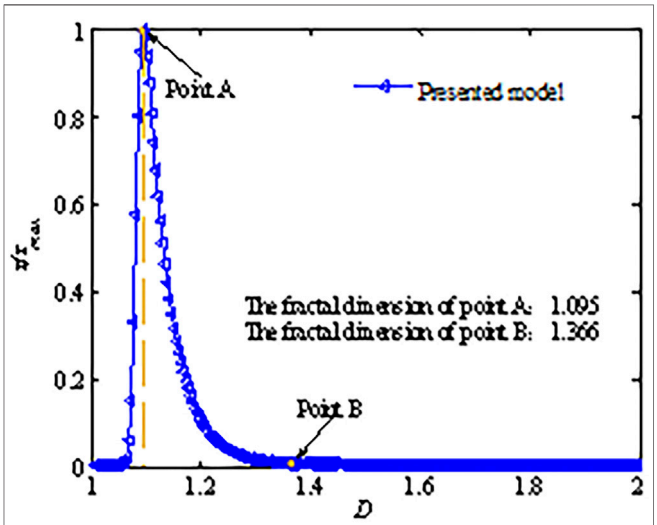

FIGURE 7 | Relationship between the shear strength and the fractal dimension *D*.

shear when $D < 1.095$. The dislocation form of asperities gradually evolves from slipping to interlocking with increasing fractal dimension. The dislocation form of the asperities on the interface is dominated by interlocking. The more asperities tend to be interlocked. As a result, the shear strength of the interface increases. When $D > 1.095$, the increase of interface roughness means the decrease of asperity base area and the asperity is easier to cut off. The dislocation form of asperity gradually evolves from interlocking to cutting off. The dislocation form of the asperities on the interface is dominated by cutting off with increasing fractal dimension. The number of interlocking asperities decreases. Therefore, the shear strength of the interface decreases. When $D = 1.095$, there are most interlocking asperities on the interface and the interlocking effect reaches the maximum. Thereby, the shear strength of interface peaks at this fractal dimension. Noted that it is the critical point of transformation of the main dislocation form from interlocking to cutting off. The cutting off of the asperities is related to the parameters of the weak material.

There is slightly difference between the presented model and the two-body mechanistic model. Analysis shows that the interface roughness is described by only the fractal dimension *D* in the two-body mechanical model, ignoring the amplitude of the asperities on the interface, namely, the parameter *G*. The fractal dimension *D* is known to determine only the frequency of occurrence for the large and small asperities on the interface. The developed model considers the influence of the asperity amplitude on the shear strength of the interface. It should be emphasized that, the number, $D = 1.095$ in **Figure 6**, is to show that the results of the presented model are consistent with the two-body mechanistic model, demonstrating the feasibility of the presented model.

However, the two-body mechanistic model obtained the shear strength evolution laws when the fractal dimension is in the range of 1~1.12 only. **Figure 7** shows the complete relationship between the interface shear strength and the fractal dimension as the fractal dimension increases from 1 to 2 based on the presented model. When $D > 1.366$, the change in the fractal dimension has little effect on the shear strength, namely, the shear strength basically remains constant when $D > 1.366$, indicated by point B in **Figure 7**.

DISCUSSION

The direct shear test results with the backfill-rock combination indicate that the interface friction angle can be larger or smaller than that of the backfill. However, the interface adhesion is always less than that of the backfill (Fall and Nasir, 2010; Koupouli et al., 2016; Fang and Fall, 2018).

Analysis suggests that the reasons for the contradictory friction angle results of the direct shear tests are mainly related to the difference in the strength of the contact

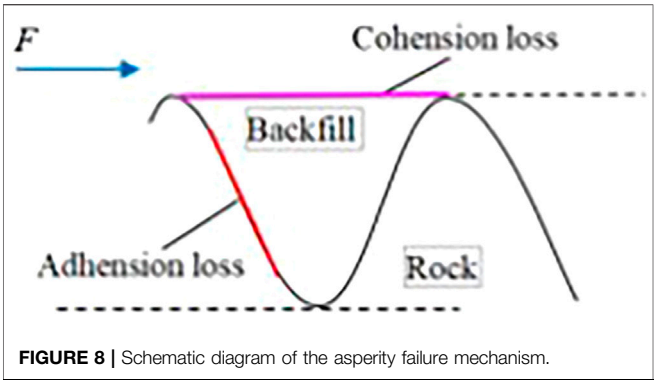

FIGURE 8 | Schematic diagram of the asperity failure mechanism.

materials and the inclined angle of the asperities on the rock surface. The interface friction angle is larger than that of backfill, if $\tan\phi_2 > 2\tan(\phi_1 + i)$, as described by **Eq. 36**. If $\tan\phi_2 < 2\tan(\phi_1 + i)$, the interface friction angle is smaller than that of the backfill.

Meanwhile, it is known that the ability of one material to adhere to the surface of another material remains constant. However, the areas providing the adhesion are not the same in different deformation regimes. The interface adhesion can be explained by the schematic diagram of the asperity failure mechanism, as shown in **Figure 8**. At the beginning, the two asperities come into locking. Adhesion is provided by the asperity surfaces when the asperities undergo elastic deformation. Then, the two asperities undergo dilatation with loading, separating on the backside of the interface relative to the direction of motion, as shown by the red line in **Figure 7**. Thus, the area providing adhesion decreases. Finally, the asperity in the backfill is cut off, and the area providing adhesion disappears completely. In summary, the interface adhesion is smaller than that of backfill, which is consistent with the experimental trend.

CONCLUSION

The original M-B fractal model is modified. A model of backfill-rock interface strength is proposed based on the modified M-B fractal model and the Mohr-Coulomb criterion. After verification, the following conclusions are obtained:

1) Based on fractal theory, a strength model that can reasonably describe the shear mechanical behavior of interfaces with random roughness is developed when materials with different strength come into contact. The deformation mechanism of the interface and the interaction of the asperities can be considered in this model.
2) The relationship between the strength parameters of the interface and that of the backfill is obtained. When the tangent of the rock friction angle is larger than twice that of the backfill, the interface friction angle is larger than that of the backfill. Otherwise, the interface friction angle is smaller than that of the backfill.
3) The shear strength of the interface changes nonlinearly with increasing fractal dimension. The shear strength increases with increasing fractal dimension when $D < 1.095$. The shear strength peaks when $D = 1.095$. The shear strength decreases with increasing fractal dimension when $D > 1.095$. Meanwhile, the shear strength basically remains constant when $D > 1.366$.

In this model, the interface shear strength is related to the interface fractal dimension and the strength parameters of the two contacting materials. In practical application, the interface roughness and the strength of the surrounding rock can be measured. The backfill strength corresponding to the maximum shear strength of the interface is obtained by this model, ensuring the stability of the underground backfill system. However, it should be noted that, the model still has some limitations that need to be solved in the future. The three-dimensional strength model of the interface is beyond the scope of this research and will continue to explore in the future. The proposed model should satisfy the assumption of the M-B fractal model, that the contact between two rough surfaces is approximately equivalent to the contact between a rough surface and a rigid flat plane. Therefore, the model is more suitable for solving the contact problem between materials with large differences in strength. Moreover, when the fractal model of the interface is established, the contact area and contact load during elastoplastic deformation are derived from the proportion of elastic and plastic deformation. The size distribution of the microcontact areas during elastoplastic deformation is assumed to be the same as that during plastic deformation. Therefore, further research on elastoplastic deformation is needed.

DATA AVAILABILITY STATEMENT

The original contributions presented in the study are included in the article/Supplementary Material, further inquiries can be directed to the corresponding author.

AUTHOR CONTRIBUTIONS

YZ developed the model and wrote the first draft of the manuscript. ZZ, LG, and XD provided constructive discussions and contributed to manuscript revision. YZ, ZZ, and LG contributed significantly to the design of the study. All authors agree to be accountable for the content of this work.

FUNDING

This research was supported by the Key Program of National Natural Science Foundation of China (No.52130905).

ACKNOWLEDGMENTS

The reviewers are gratefully acknowledged for their constructive comments.

REFERENCES

Beheshti, A., and Khonsari, M. M. (2014). On the Contact of Curved Rough Surfaces: Contact Behavior and Predictive Formulas. *J. Appl. Mech.* 81 (11), 111004. doi:10.1115/1.4028426

Belem, T., and Benzaazoua, M. (2008). Design and Application of Underground Mine Paste Backfill Technology. *Geotech. Geol. Eng.* 26, 147–174. doi:10.1007/s10706-007-9154-3

Berry, M. V., and Lewis, Z. V. (1980). On the Weierstrass-Mandelbrot Fractal Function. *Proc. R. Soc. Lond. A.* 370, 459–484. doi:10.1098/rspa.1980.0044

Carbone, G. (2009). A Slightly Corrected Greenwood and Williamson Model Predicts Asymptotic Linearity between Contact Area and Load. *J. Mech. Phys. Sol.* 57 (7), 1093–1102. doi:10.1016/j.jmps.2009.03.004

Chen, X., Shi, X., Zhou, J., Chen, Q., Li, E., and Du, X. (2018). Compressive Behavior and Microstructural Properties of Tailings Polypropylene Fibre-Reinforced Cemented Paste Backfill. *Construction Building Mater.* 190, 211–221. doi:10.1016/j.conbuildmat.2018.09.092

Cui, L., and Fall, M. (2017). Multiphysics Modeling of Arching Effects in Fill Mass. *Comput. Geotechnics* 83, 114–131. doi:10.1016/j.compgeo.2016.10.021

Fall, M., Benzaazoua, M., and Ouellet, S. (2005). Experimental Characterization of the Influence of Tailings Fineness and Density on the Quality of Cemented Paste Backfill. *Minerals Eng.* 18 (1), 41–44. doi:10.1016/j.mineng.2004.05.012

Fall, M., and Nasir, O. (2010). Mechanical Behaviour of the Interface between Cemented Tailings Backfill and Retaining Structures under Shear Loads. *Geotech. Geol. Eng.* 28 (6), 779–790. doi:10.1007/s10706-010-9338-0

Fang, K., Cui, L., and Fall, M. (2020). A Coupled Chemo-Elastic Cohesive Zone Model for Backfill-Rock Interface. *Comput. Geotechnics* 125, 103666. doi:10.1016/j.compgeo.2020.103666

Fang, K., and Fall, M. (2019). Chemically Induced Changes in the Shear Behaviour of Interface between Rock and Tailings Backfill Undergoing Cementation. *Rock Mech. Rock Eng.* 52, 3047–3062. doi:10.1007/s00603-019-01757-0

Fang, K., and Fall, M. (2018). Effects of Curing Temperature on Shear Behaviour of Cemented Paste Backfill-Rock Interface. *Int. J. Rock Mech. Mining Sci.* 112, 184–192. doi:10.1016/j.ijrmms.2018.10.024

Ghirian, A., and Fall, M. (2013). Coupled Thermo-Hydro-Mechanical-Chemical Behaviour of Cemented Paste Backfill in Column Experiments. Part I: Physical, Hydraulic and thermal Processes and Characteristics. *Eng. Geology.* 164, 195–207. doi:10.1016/j.enggeo.2013.01.015

Greenwood, J. A., and Williamson, J. B. P. (1966). Contact of Nominally Flat Surfaces. *Proc. R. Soc. Lond. A.* 295 (1442), 300–319. doi:10.1098/rspa.1966.0242

Hill, R. (1950). *The Mathematical Theory of Plasticity*. London: Oxford University Press.

Jackson, R. L., and Green, I. (2003). A Finite Element Study of Elasto-Plastic Hemis- Pherical Contact against a Rigid Flat. *J. Tribol.-T. ASME* 127 (2), 343–354. doi:10.1115/2003-TRIB-0268

Jiang, H.-q., Fall, M., Li, Y.-H., and Han, J. (2019). An Experimental Study on Com-Pressive Behavior of Cemented Rockfill. *Constr. Build. Mater.* 147, 837–846. doi:10.1016/j.conbuildmat.2019.04.061

Jiang, H., and Fall, M. (2017). Yield Stress and Strength of saline Cemented Tailings Materials in Sub-zero Environments: Slag-Paste Backfill. *J. Sust. Cement-Based Mater.* 6 (5), 314–331. doi:10.1080/21650373.2017.1280428

Johnson, K. L. (1985). *Contact Mechanics*. Cambridge: Cambridge University Press.

Kogut, L., and Etsion, I. (2002). Elastic-Plastic Contact Analysis of a Sphere and a Rigid Flat. *J. Appl. Mech.-T ASME* 69 (5), 657–662. doi:10.1115/1.1490373

Koupouli, N. J. F., Belem, T., Rivard, P., and Effenguet, H. (2016). Direct Shear Tests on Cemented Paste Backfill-Rock Wall and Cemented Paste Backfill-Backfill Interfaces. *J. Rock Mech. Geotechnical Eng.* 8, 472–479. doi:10.1016/j.jrmge.2016.02.001

Li, L., and Aubertin, M. (2015). Numerical Analysis of the Stress Distribution in Symmetrical Backfilled Trenches with Inclined Walls. *Indian Geotech. J.* 45 (3), 278–290. doi:10.1007/s40098-014-0131-5

Li, Y., Liu, W., Yang, C., and Daemen, J. J. K. (2014). Experimental Investigation of Mechanical Behavior of Bedded Rock Salt Containing Inclined Interlayer. *Int. J. Rock Mech. Mining Sci.* 69, 39–49. doi:10.1016/j.ijrmms.2014.03.006

Lingga, B. A., and Apel, D. B. (2018). Shear Properties of Cemented Rockfills. *J. Rock Mech. Geotechnical Eng.* 10 (4), 635–644. doi:10.1016/j.jrmge.2018.03.005

Liou, J. L., Tsai, C. M., and Lin, J.-f. (2010). A Microcontact Model Developed for Sphere- and cylinder-based Fractal Bodies in Contact with a Rigid Flat Surface. *Wear* 268, 431–442. doi:10.1016/j.wear.2009.08.033

Liu, G., Li, L., Yang, X., and Guo, L. (2016). A Numerical Analysis of the Stress Distribution in Backfilled Stopes Considering Nonplanar Interfaces between the Backfill and Rock Walls. *Int. J. Geotechnical Eng.* 10 (3), 271–282. doi:10.1080/19386362.2015.1132123

Liu, G., Li, L., Yang, X., and Guo, L. (2017). Numerical Analysis of Stress Distribution in Backfilled Stopes Considering Interfaces between the Backfill and Rock Walls. *Int. J. Geomech.* 17 (2), 06016014. doi:10.1061/(ASCE)GM.1943-5622.0000702

Liu, P., Zhao, H., Huang, K., and Chen, Q. (2015). Research on Normal Contact Stiffness of Rough Surface Considering Friction Based on Fractal Theory. *Appl. Surf. Sci.* 349, 43–48. doi:10.1016/j.apsusc.2015.04.174

Liu, X.-r., Zhou, H.-w., and Li, H. (2005). Numerical Simulation of Interface Behavior in Rock-Concrete Interaction Problem. *Chin. J. Rock Mech. Eng.* 24 (S2), 5648–5651. CNKI:SUN:YSLX.0.2005-S2-065.

Luo, L., Li, X., Tao, M., and Dong, L. (2017). Mechanical Behavior of Rock-Shotcrete Interface under Static and Dynamic Tensile Loads. *Tunnelling Underground Space Tech.* 65, 215–224. doi:10.1016/j.tust.2017.03.005

Majumdar, A., and Bhushan, B. (1991). Fractal Model of Elastic-Plastic Contact between Rough Surfaces. *J. Tribol.* 113 (1), 1–11. doi:10.1115/1.2920588

Majumder, A., and Tien, C. L. (1990). Fractal Characterization and Simulation of Rough Surfaces. *Wear* 136 (2), 313–327. doi:10.1016/0043-1648(90)90154-3

Mandelbrot, B. B. (1985). Self-Affine Fractals and Fractal Dimension. *Phys. Scr.* 32, 257–260. doi:10.1088/0031-8949/32/4/001

Maruschak, P. O., Konovalenko, I. V., and Bishchak, R. T. (2012). Effect of Thermal Fatigue Cracks on Brittle-Ductile Deformation and Failure of Cbcm Roller Surface Layers. *Metallurgist* 56 (1-2), 30–36. doi:10.1007/s11015-012-9532-9

Morag, Y., and Etsion, I. (2007). Resolving the Contradiction of Asperities Plastic to Elastic Mode Transition in Current Contact Models of Fractal Rough Surfaces. *Wear* 262 (5), 624–629. doi:10.1016/j.wear.2006.07.007

Sayles, R. S., and Thomas, T. R. (1978). Surface Topography as a Nonstationary Random Process. *Nature* 271 (2), 431–434. doi:10.1038/271431a0

Selçuk, L., and Aşma, D. (2019). Experimental Investigation of the Rock-Concrete Bi Materials Influence of Inclined Interface on Strength and Failure Behavior. *Int. J. Rock Mech. Mining Sci.* 123, 1–11. doi:10.1016/j.ijrmms.2019.104119

Sivakugan, N., Widisinghe, S., and Wang, V. Z. (2013). Vertical Stress Determination within Backfilled Mine Stopes. *Int. J. Geomech.* 14 (5), 1–5. doi:10.1061/(ASCE)GM.1943-5622

Tariq, A., and Yanful, E. K. (2018). A Review of Binders Used in Cemented Paste Tailings for Underground and Surface Disposal Practices. *J. Environ. Manage.* 131, 138–149. doi:10.1016/j.jenvman.2013.09.039

Ting, C. H., Sivakugan, N., Read, W., and Shukla, S. K. (2014). Analytical Expression for Vertical Stress within an Inclined Mine Stope with Non-parallel Walls. *Geotech. Geol. Eng.* 32 (2), 577–586. doi:10.1007/s10706-014-9735-x

Weilv, W., Xu, W., and Jianpin, Z. (2021). Effect of Inclined Interface Angle on Shear Strength and Deformation Response of Cemented Paste Backfill-Rock under Triaxial Compression. *Construction Building Mater.* 279, 122478. doi:10.1016/j.conbuildmat.2021.122478

Zhao, Y., Maietta, D. M., and Chang, L. (2000). An Asperity Microcontact Model Incorporating the Transition from Elastic Deformation to Fully Plastic Flow. *J. Tribol.* 122, 86–93. doi:10.1115/1.555332

Conflict of Interest: The authors declare that the research was conducted in the absence of any commercial or financial relationships that could be construed as a potential conflict of interest.